Efficient radical-based light-emitting diodes with doublet emission

Xin Ai,[1†] Emrys W. Evans,[2†] Shengzhi Dong,[1†] Alexander J. Gillett,[2] Haoqing Guo,[1] Yingxin Chen,[1] Timothy J. H. Hele,[2] Richard H. Friend, [2] and Feng Li[1,2*]*

[1]*State Key Laboratory of Supramolecular Structure and Materials, College of Chemistry, Jilin University, Qianjin Avenue 2699, Changchun, 130012, P. R. China*
[2]*Cavendish Laboratory, University of Cambridge, JJ Thomson Avenue, Cambridge, CB3 0HE, United Kingdom*

† These authors contributed equally to this work.
* Author to whom correspondence should be addressed;
E-mail: rhf10@cam.ac.uk, lifeng01@jlu.edu.cn

Organic light-emitting diodes (OLEDs),[1-5] quantum-dot-based LEDs (QLEDs),[6-10] perovskites-based LEDs[11-13] and micro-LEDs[14,15] are in competition to provide the basis for next-generation displays and active lighting, all offering attractive prospects for lightweight and flexible units. Here we demonstrate efficient operation of radical-based OLEDs,[16] in which the emission comes from a spin doublet rather than a singlet or triplet exciton. Whilst the emission process is still spin-allowed in these systems, usefully, the classical triplet-limiting efficiency for OLEDs is circumvented for doublets. Using a luminescent radical emitter, we demonstrate an OLED with maximum external quantum efficiency (EQE) of 27% at a wavelength of 710 nm – this being the highest reported value for deep-red/infrared LEDs. For a standard closed-shell organic semiconductor, hole and electron states involve occupancy of highest-occupied- and lowest-unoccupied molecular orbital, HOMO and LUMO, and recombine to form singlet or triplet exciton states. Radical emitters have a singly-occupied molecular orbital (SOMO) in the ground state, giving an overall spin-1/2 doublet. If as expected on energetic grounds, both electron and hole occupy this SOMO level, recombination returns the system to the ground state, giving no light emission. However, in our very efficient LEDs, we achieve selective hole injection into the HOMO and electron injection to the SOMO.

For the most part, stable, organic luminescent radicals have posed as curiosities of chemistry with limited applications.[17-23] Photoexcitation of doublet ground state (D_0) molecules generate doublet excited states. Spin-allowed emission, i.e. fluorescence, in these molecules originates from the lowest-lying doublet excited state, D_1 (Fig. 1a).

By incorporating 3-substituted-9-(naphthalen-2-yl)-9H-carbazole (3NCz) and 3-substituted-9-phenyl-9H-carbazole (3PCz) to the core tris(2,4,6-trichlorophenyl)methyl (TTM) radical, we obtained two new luminescent radicals, TTM-3NCz and TTM-3PCz (Fig. 1b). The photoluminescence quantum efficiency (PLQE) values in solid 4,4-bis(carbazol-9-yl)biphenyl CBP matrix film (3.0% wt) are 85.6 ± 5.4% and 60.4 ± 0.9% for deep-red emission in TTM-3NCz

(707 nm) and TTM-3PCz (695 nm), respectively, and can be translated to excellent device performance. See dashed lines in Fig. 1c for the photoluminescence spectra (photoexcitation at 375 nm).

A series of OLEDs were made using TTM-3NCz and TTM-3PCz as emitters by vacuum deposition processing (pressure < 6×10^{-7} Torr). The evaporation temperatures of TTM-3NCz and TTM-3PCz under vacuum are below 473 K, which are much lower than their respective thermal decomposition temperatures of 635 K and 640 K (Extended Data, Fig. 1a), meaning that their thermal stabilities are sufficient to withstand the thermal-evaporation process. The energy levels of the two compounds were obtained from cyclic voltammetry (CV) measurements (Extended Data, Fig. 2a, 2c). Furthermore, in order to assess the electrochemical stabilities of TTM-3NCz and TTM-3PCz, we scanned 20 cycles of CV curves (Extended Data, Fig. 2b, 2d). There are no significant changes between curves, which indicates good redox stability for TTM-3NCz and TTM-3PCz (in addition to good photo-stability, Extended Data, Fig. 3).

1-Bis[4-[N,N-di(4-tolyl)amino]phenyl]cyclohexane (TAPC)[1] and 2,4,6-tris[m-(diphenylphosphinoyl)phenyl]-1,3,5-triazine (POT2T)[24] were used as 35 nm hole- and 70 nm electron-transporting layers, respectively. The radicals were doped into a CBP host to form the light-emitting layer (thickness 25–40 nm). Due to the larger energy band gap of CBP when compared to the dopant molecules, see Fig. 1d inset, sequential charge trapping is expected to be the main route for the creation of doublet excitons. A thin layer (10 nm) of 4,6-Bis(3,5-di(pyridin-3-yl)phenyl)-2-methylpyrimidine (B3PYMPM)[25] was inserted between light-emitting and PO-T2T layers to remove unwanted green emission (likely CBP:PO-T2T exciplex). Best LED performance was found to be ITO/MoO_3 (3 nm)/TAPC (35 nm)/CBP:TTM-3NCz (3.0 wt %) (40 nm) or CBP:TTM-3PCz (3.0 wt %) (25 nm)/B3PYMPM (10 nm)/PO-T2T (70 nm)/LiF (0.8 nm)/Al (100 nm).

Plots of EQE against current density for the OLEDs are given in Fig. 1d (TTM-3NCz = red, TTM-3PCz = black). The corresponding electroluminescence (EL) spectra peak at 710 nm (TTM-3NCz) and 703 nm (TTM-3PCz); the devices have true deep-red/near-infrared emission (Fig. 1c). Maximum EQE values of 27 ± 5% for TTM-3NCz and 17 ± 3% for TTM-3PCz OLEDs suggest near 100% internal quantum efficiency (IQE) for electroluminescence when considered with the film PLQE values and a 30% light-out-coupling coefficient.[5] To the best of our knowledge, the maximum EQE of TTM-3NCz-based device is the highest value for all deep-red/infrared LEDs [26-28] (see Table S2), and respectable > 10 % EQE values are obtained at 1 mA/cm^2. The near-identical EL and PL spectra (Fig.1 c) for TTM-3NCz and TTM-3PCz show that EL and PL emission originate from the same electronic transition ($D_1 \rightarrow D_0$).

Current density-voltage-EL characteristics for the TTM-3NCz and TTM-3PCz-based devices are given in Fig. 1e and 1f. The plot positions associated with the maximum EQE values are denoted by arrows and occur in the device turn-on regions, above the experimental noise levels. Besides the performance of the champion devices shown in Fig. 1, the performance of another five TTM-3NCz (EQE_{max} = 27–16 %) devices are shown in Extended Data, Fig. 4. The EL spectra are unchanged for a wide range of operating current densities: 6 μA/cm^2–1.6 mA/cm^2 (Extended Data, Fig. 5).

We note that TTM-3NCz and TTM-3PCz contain ‘donor’-3NCz/-3PCz and ‘acceptor’-TTM radical groups which resemble the classical TADF motif. In Fig. 2a absorption and photoluminescence spectra for the molecules are plotted with reference to TTM. Introduction of the ‘donor’ group to the TTM moiety leads to the appearance of a new absorption band at ~620 nm and an accompanying ~0.38 eV red shift in PL. High ‘charge transfer’-CT character is expected for the first excited state of TTM-3NCz and TTM-3PCz, i.e. significant spatial separation with little overlap for the -3NCz/-3PCz-centred-highest occupied molecular orbital (HOMO) and TTM-centred-singly occupied molecular orbital (SOMO). These frontier molecular

orbitals (MOs) can be used to describe electronic transitions for ground state (D_0) absorption to the lowest excited state (D_1) and in photo- and electro-luminescence ($D_1 \rightarrow D_0$). The same (δ^-)TTM–donor(δ^+) dipole moment orientation is expected for D_1 versus D_0, but with greater magnitude in the excited state. This is supported by the observation of strong, positive solvatochromic effects (see Fig. 2a, 2b: photoexcitation at 375 nm). Increasing the solvent polarizability index leads to increasing Stokes' shifts. The slope for the Lippert-Mataga plot of the TTM-3NCz molecules in Fig. 2c reflects the change in dipole moment ($\Delta\delta$) upon photoexcitation, and shows a fitting contrast with the solvent-independent behaviour (i.e. $\Delta\delta \sim 0$) for TTM. In TTM the D_1 excited state is more local excited-'LE' in nature (i.e. significant HOMO/SOMO overlap).

It is critical that the dopant emitters possess high PLQE for good LED performance. PLQE values of 49% and 46% are obtained for toluene solutions of TTM-3NCz and TTM-3PCz, respectively. The Energy Gap Law generally precludes efficient deep-red/infrared light emission but does not appear to be strictly followed for dopants with appreciable CT-character in emission.[27] In favour of OLEDs, the non-radiative decay pathways were found to be further reduced when 3% wt doped in CBP films, giving rise to the PLQE values of 90% (TTM-3NCz) and 61% (TTM-3PCz) which were reported above.

To explore the nature of the doublet excited states, we performed nanosecond transient absorption (TA) and PL (trPL) studies on toluene solutions containing TTM-3NCz and TTM-3PCz. Excitation wavelengths of 532 nm and 600 nm were used for TA and trPL, respectively, and chosen so to excite the broad absorption band associated with the $D_0 \rightarrow D_1$ transition. In the ns-trPL measurements, we observe an emission spectrum that closely resembles the steady-state PL for TTM-3NCz and TTM-3PCz. There is no temporal evolution in the spectra. Furthermore, from the overlaid TA and trPL profiles (Fig. 2d), it is apparent that there are no excited state species living beyond the emission lifetime. Whilst dark, triplet states usually occur at lower energy than emissive singlet states for closed-shell systems, we consider that

there are no equivalent triplet states to hinder emission for the open-shell TTM-3NCz and TTM-3PCz molecules. Further discussion of the transient absorption measurements can be found in SI 2.

The PL kinetics can be fitted with a mono-exponential function to yield lifetimes of 17.2 ns (TTM-3NCz) and 21.2 ns (TTM-3PCz). In combination with the PLQE values, the radiative decay rates are: TTM-3NCz = 2.9×10^7 s^{-1}, TTM-3PCz = 2.1×10^7 s^{-1}. These values are an order of magnitude larger than those associated with delayed emission from typical TADF molecules (ca. 2,4,5,6-tetra(9H-carbazol-9-yl)isophthalonitrile, 4CzIPN). This is particularly important for LEDs as higher radiative rates mean reduced exciton-charge annihilation issues in efficiency roll-off.

Finally, the molecular properties and photophysics for TTM-3NCz/TTM-3Cz molecules can be reconciled with density functional theory calculations. Using UKS-DFT and UKS-TDDFT with B3LYP functional and 6-31G** basis set, the nature of the electronic states is revealed. We interpret the computational results within the MO diagram shown in Figure 3a. The scheme begins with TTM and considers interactions between benzene HOMO/LUMO moieties and the central carbon $2p_z$ orbital. A relatively strong, 374–378 nm absorption peak found for TTM and TTM-donor-type molecules is attributed to a SOMO → LUMO transition. The SOMO has electron density on every other atom of the TTM group, and can be determined from first principles, along with the overall HOMO, as outlined in SI 3 using group- and Hückel theory. The derived SOMO has the same form as obtained by DFT (Fig. 3b). In TTM, TTM-3NCz and TTM-3PCz, the overall LUMO mirrors the LUMO of the -TTM benzene groups (Fig. 3a).

HOMO → SOMO transitions give rise to the lowest energy absorption bands in both TTM-3NCz (616 nm) and TTM (541 nm) in toluene, with significant CT- and LE-character for the former and latter types. This arises as the TTM-3NCz/TTM-3PCz HOMOs are primarily hybrids of the most anti-bonding

combinations of -TTM and carbazole-group HOMOs (Fig. 3b). On going from TTM to TTM-3NCz, the TTM MO diagram is perturbed as depicted in Fig. 3a. Unexpectedly good agreement is found between the absorption spectra and UKS-TDDFT peak positions[29] in TTM-3NCz: HOMO → SOMO, experimental = 616 nm, calculated = 622 nm. More detailed discussions of the MO diagram and electronic structure calculations can be found in SI 3 and 4.

The SOMO → HOMO transitions as depicted in Fig. 3b are associated with luminescence. However, whilst the route to efficient doublet emission for the open-shell molecules must involve these orbitals, thermodynamics would dictate that electrons and holes are both stabilized by occupancy of the SOMO level following electrical injection (see Fig. 4a). It would not be possible to realize doublet excited states for light emission by this scheme.

As shown in Fig. 1d (inset), the electrodes are biased for selective hole and electron injection into the -3NCz/-3PCz HOMO and -TTM SOMO levels, respectively (ca. Energy Gap Law). If injection of the hole into the HOMO occurs before the electron into the SOMO, positively charged, singlet and triplet intermediates are expected (see Fig. 4b). It is possible that the positively charged singlet intermediate for the former case could 'relax' before the electron falls upon the SOMO, but this loss pathway to D_1-formation is spin forbidden for the triplet intermediates. On the other hand, if injection of the electron into the SOMO occurs first, this gives the negatively charged singlet intermediate also shown in Fig. 4b. In this second scenario, holes that travel via CBP HOMO levels, could encounter negatively-charged TTM-3NCz sites to form D_1 by tunnelling of the hole between the carbazoles of CBP and TTM-3NCz. The hole could also hop between TTM-3NCz sites, when avoiding the aforementioned singlet 'relaxation'. To date, it is noteworthy that TTM-donor-type molecules have been found to make much better OLEDs than TTM,[30] and thereby provides some indirect evidence for the mechanism in Fig. 4b.

The discussion in Fig. 4b considers hole injection sequentially to the CBP host and then onto the TTM-3NCz HOMO level. We can also consider models for operation without participation of the CBP in which charge annihilation of TTM-3NCz anions and cations generates the same D_1 excited state. This would require that energy levels are substantially lowered and raised following oxidation and reduction, respectively, so that the TTM-3NCz cation 'SOMO' and anion 'HOMO' would become more favourably aligned for electron transfer to yield $D_0 + D_1$, as illustrated schematically in Fig. 4c. Though energy shifts on charging are expected, indications from cyclic voltammetry (Extended Data, Fig. 2) suggest these shifts are too small to achieve the level alignment indicated in Fig. 4c.

At this stage, the precise route from electrical injection to luminescence is unclear but appears to be, undoubtedly, efficient.

In this work, we have demonstrated highly efficient radical-based OLEDs with EQE values which far exceed those for other LEDs with deep-red/near-IR emission. Our scheme is based on using open-shell, doublet dopants which undergo emission following donor-radical charge-transfer. The SOMO in these molecules facilitates exceptional LED performance and its novel spin properties offer many possibilities for exploitation in other fields of optoelectronics.

1 Tang, C. W. & VanSlyke, S. A. Organic electroluminescent diodes. *Appl. Phys. Lett.* **51**, 913-915 (1987).

2 Burroughes, J. H. *et al.* Light-emitting diodes based on conjugated polymers. *Nature* **347**, 539-541 (1990).

3 Baldo, M. A. *et al.* Highly efficient phosphorescent emission from organic electroluminescent devices. *Nature* **395**, 151-154 (1998).

4 Ma, Y., Zhang, H., Shen, J. & Che, C. Electroluminescence from triplet metal-ligand charge-transfer excited state of transition metal complexes. *Synthetic Met.* **94**, 245-248 (1998).

5 Uoyama, H., Goushi, K., Shizu, K., Nomura, H. & Adachi, C. Highly efficient organic light-emitting diodes from delayed fluorescence. *Nature* **492**, 234-238 (2012).

6 Tessler, N., Medvedev, V., Kazes, M., Kan, S. & Banin, U. Efficient near-infrared polymer nanocrystal light-emitting diodes. *Science* **295**, 1506-1508, (2002).

7 Sun, Q. *et al.* Bright, multicoloured light-emitting diodes based on quantum dots. *Nature Photon.* **1**, 717-722 (2007).

8 Dai, X. *et al.* Solution-processed, high-performance light-emitting diodes based on quantum dots. *Nature* **515**, 96-99 (2014).

9 Yang, Y. *et al.* High-efficiency light-emitting devices based on quantum dots with tailored nanostructures. *Nature Photon.* **9**, 259-266 (2015).

10 Dai, X., Deng, Y., Peng, X. & Jin, Y. Quantum-dot light-emitting diodes for large-area displays: towards the dawn of commercialization. *Adv. Mater.* **29**, 1607022 (2017).

11 Tan, Z.-K. *et al.* Bright light-emitting diodes based on organometal halide perovskite. *Nature Nanotech.* **9**, 687-692 (2014).

12 Cho, H. *et al.* Overcoming the electroluminescence efficiency limitations of perovskite light-emitting diodes. *Science* **350**, 1222-1225, (2015).

13 Wang, N. *et al.* Perovskite light-emitting diodes based on solution-processed self-organized multiple quantum wells. *Nature Photon.* **10**, 699-704, (2016).

14 Jin, S., Li, J., Li, J., Lin, J. & Jiang, H. GaN microdisk light emitting diodes. *Appl. Phys. Lett.* **76**, 631-633 (2000).

15 Zhang, K., Peng, D., Lau, K. M. & Liu, Z. Fully-integrated active matrix programmable UV and blue micro-LED display system-on-panel (SoP). *J. Soc. Inf. Display* **25**, 240-248, (2017).

16 Peng, Q., Obolda, A., Zhang, M. & Li, F. Organic light-emitting diodes using a neutral π radical as emitter: the emission from a doublet. *Angew. Chem., Int. Ed.* **54**, 7091-7095 (2015).

17 Ballester, M., Molinet, C. & Castañer, J. Preparation of highly strained aromatic chlorocarbons. I. A powerful nuclear chlorinating agent. Relevant reactivity phenomena traceable to molecular strain. *J. Am. Chem. Soc.* **82**, 4254-4258 (1960).

18 Armet, O. *et al.* Inert carbon free radicals. 8. Polychlorotriphenylmethyl radicals: synthesis, structure, and spin-density distribution. *J. Phys. Chem.* **91**, 5608-5616 (1987).

19 Heckmann, A., Lambert, C., Goebel, M. & Wortmann, R. Synthesis and photophysics of a neutral organic mixed-valence compound. *Angew. Chem., Int. Ed.* **43**, 5851-5856 (2004).

20 Velasco, D. *et al.* Red organic light-emitting radical adducts of carbazole and tris(2,4,6-trichlorotriphenyl)methyl radical that exhibit high thermal stability and electrochemical amphotericity. *J. Org. Chem.* **72**, 7523-7532 (2007).

21 Castellanos, S., Velasco, D., López-Calahorra, F., Brillas, E. & Julia, L. Taking advantage of the radical character of tris(2,4,6-trichlorophenyl)methyl to synthesize new paramagnetic glassy molecular materials. *J. Org. Chem.* **73**, 3759-3767 (2008).

22 Hattori, Y., Kusamoto, T. & Nishihara, H. Luminescence, stability, and proton response of an open-shell (3,5-dichloro-4-pyridyl)bis(2,4,6-trichlorophenyl)methyl radical. *Angew. Chem., Int. Ed.* **53**, 11845-11848 (2014).

23 Ai, X., Chen, Y., Feng, Y. & Li, F. A stable room-temperature luminescent biphenylmethyl radical. *Angew. Chem., Int. Ed.* **57**, 2869-2873, (2018).

24 Hung, W. Y. *et al.* The first tandem, all-exciplex-based WOLED. *Sci. Rep.* **4**, 5161 (2014).

25 Sasabe, H. *et al.* 2-Phenylpyrimidine skeleton-based electron-transport materials for extremely efficient green organic light-emitting devices. *Chem. Commun.* 5821-5823 (2008).

26 Li, C. *et al.* Deep-red to near-infrared thermally activated delayed fluorescence in organic solid films and electroluminescent devices. *Angew. Chem., Int. Ed.* **56**, 11525-11529 (2017).

27 Kim, D.-H. *et al.* High-efficiency electroluminescence and amplified spontaneous emission from a thermally activated delayed fluorescent near-infrared emitter. *Nature Photon.* **12**, 98-104 (2018).

28 Xue, J. *et al.* High-Efficiency Near-Infrared Fluorescent Organic Light-Emitting Diodes with Small Efficiency Roll-Off: A Combined Design from Emitters to Devices. *Adv. Funct. Mater.* **27**, 1703283 (2017).

29 Ipatov, A. et al. Excited-state spin-contamination in time-dependent density-functional theory for molecules with open-shell ground states. J. Mol. Struct.: THEOCHEM 914, 60-73 (2009).

30 Neier, E. *et al.* Solution-processed organic light-emitting diodes with emission from a doublet exciton; using (2,4,6-trichlorophenyl)methyl as emitter. *Org. Electron.* **44**, 126-131 (2017).

Acknowledgements

X.A., S.D., H.G., Y.C. and F.L. are grateful for the financial support received from National Key R&D Program of China (Grant No. 2016YFB0401001), National Natural Science Foundation of China (Grant No. 51673080, 91233113), and National Key Basic Research and Development Program of China (973 program, Grant No. 2015CB655003). E.W.E., A.J.G. and R.H.F. would like to thank the EPSRC for funding this work (EP/M01083X/1, EP/M005143/1). T.J.H.H. thanks Jesus College, Cambridge for a Research Fellowship. F.L. is an academic visitor at the Cavendish Laboratory, Cambridge, and is supported by the China Scholarship Council (CSC) and the Talents Cultivation Program (Jilin University, China).

Author Statements

X.A., S.D. and H.G. designed and synthesized the luminescent radicals, and performed the steady-state spectroscopy. E.W.E. performed the transient photoluminescence (trPL) measurements and the quantum chemical calculations. T.J.H.H devised the group theory treatment. A.J.G. conducted the transient absorption (TA) spectroscopy measurements. X.A., Y.C. and F.L. optimized the devices.

E.W.E., R.H.F. and F.L. initiated, designed and supervised the work. E.W.E., R.H.F. and F.L. wrote the manuscript, and received input from all authors.

Correspondence and requests for materials should be addressed to R.H.F. and F.L. (rhf10@cam.ac.uk, lifeng01@jlu.edu.cn).

Figure Legends

Figure 1. **LEDs with doublet emission.** a) Doublet emission following photo- and electrical-excitation. b) Chemical structures for TTM, TTM-3NCz and TTM-3PCz. c) Electroluminescence (solid lines) and photoluminescence (dotted lines, 375 nm excitation) spectra for TTM-3NCz (red)- and TTM-3PCz (black). d) External quantum efficiency-current density (EQE-J) curves for TTM-3NCz (red) and TTM-3PCz (black) LEDs. Inset: TTM-3NCz device layout; SOMO = –3.7 V (cyclic voltammetry – Extended Data, Fig. 2) and HOMO = –6.0 V (approximated by 9-phenylcarbazole). Black triangle and red circle markers denote current density-voltage (J-V) and radiance-V profiles for e) TTM-3NCz and f) TTM-3PCz. Radiance levels corresponding to EQE_{max} lie above the background noise level.

Figure 2. **Doublet photophysics.** Steady-state a) UV-Vis and b) PL profiles for 10 μM TTM-3NCz in solvents of varying orientation polarizability index, *f*. Reference measurements for 10 μM TTM in toluene are denoted by black dotted lines. Photoexcitation wavelength = 375 nm. c) Lippert-Mataga plot of Stokes' shift versus *f* for TTM-3NCz (red circles) and TTM (black triangles). d) Overlaid kinetic profiles for PL (all-integrated, red circles; 600 nm excitation at 6.5 $\mu J/cm^2$ fluence) and transient absorption (600–700 nm averaged, black squares; 1550–1650 nm averaged, black triangles; 532 nm excitation at 35.7 $\mu J/cm^2$ fluence). Sample concentration = 10–100 μM.

Figure 3. **Electronic structure for doublets: from HOMO to SOMO.** a) Molecular orbital diagrams for TTM and TTM-3NCz. Structures are geometry optimized for the D_1 state by UKS-TDDFT (B3LYP, 6-31G**), and the molecular orbitals involved in a monoelectronic depiction for $D_1 \rightarrow D_0 + h\nu$ are shown in b).

Figure 4. **Doublet electroluminescence mechanism.** a) Scheme depicts how thermodynamically-favoured SOMO electron and hole injection does not realize the emissive doublet excited state. b) Electroluminescence by selective HOMO and SOMO hole and electron injection. c) Electroluminescence by TTM-3NCz/TTM-3PCz charge annihilation mechanism.

Methods

Synthesis of Doublet Emitters. The precursors of TTM-3NCz and TTM-3PCz were prepared by Suzuki-coupling of tris(2,4,6-trichlorophenyl)methane (HTTM) and 4,4,5,5-tetramethyl-1,3,2-dioxaborolan-2-yl-'3NCz'/'3PCz'. Radicals were generated from the precursors by treatment with potassium *t*-butoxide in tetrahydrofuran, followed by oxidation of the resulting carbanions with *p*-chloranil. Full synthesis and characterization details are described in Supplementary Information (SI) 1.2.

Device-physics. Current density-voltage-electroluminescence (J-V-EL) characteristics were measured using a Keithley 2400 sourcemeter, Keithley 2000 multimeter and a calibrated silicon photodiode.

Photo-physics. UV/Vis absorption spectra were measured on a Shimadzu UV-2550 spectrometer. Fluorescence spectra were recorded on a Shimadzu 5301PC spectrometer. The absolute fluorescence quantum yields were obtained using an Edinburgh Instruments FLS920 spectrometer with the integrating sphere method. Photoluminescence lifetimes were measured either by an Edinburgh Instruments FLS980 spectrometer (time resolution) or Andor iStar DH740 CCI-010 ICCD camera with Andor SR303i spectrograph (time and spectral resolution). Experimental details for the transient absorption measurements are given in the Supplementary Information.

Electronic Structure Calculations. For the ground state, unrestricted Kohn-Sham (UKS)-DFT calculations were performed with the Orca package (version 4.0.1) using the B3LYP functional and 6-31G** basis set. For the excited states, UKS-time-dependent DFT (UKS-TDDFT) was employed with the Tamm-Dancoff approximation. All calculations were treated in vacuo.

Data Availability Statement

The datasets underlying this work are available at DOI. [to be added in proofs].

Extended Data Figure Legends

Figure 1. **TTM-3NCz and TTM-3PCz: Thermal stability and EPR.**

a) TGA measurements show thermal decomposition temperatures of 362^{o}C (TTM-3NCz) and 367^{o}C (TTM-3PCz).

b) EPR spectra for solid samples at room temperature

Figure 2. **Electrochemical properties and stability.**

Cyclic voltammograms of a) TTM-3NCz and c) TTM-3PCz in CH_2Cl_2. For both TTM-3NCz and TTM-3PCz, average of cathodic and anodic potenials give: reduction potential = –1.1 V; first oxidation potential = +0.4 V; second oxidation potential = +0.9 V. Multi-cycle CV measurements (20 cycles) of b) TTM-3NCz and d) TTM-3PCz in CH_2Cl_2.

Figure 3. Photostability of TTM and TTM-3NCz.

Luminescence intensity plots for TTM-3NCz and TTM solutions (10 μM, cyclohexane). A pulsed laser at 355 nm with an energy density of 315 kW/cm^2 (pulse width: 8 ns; frequency: 10 Hz) was used under ambient conditions.

Figure 4. Device reproducibility for TTM-3NCz.

a) External quantum efficiency versus current density plots for five TTM-3NCz devices. Peak EQE_{max} values: 1) 25 %, 2) 27 %, 3) 20 %, 4) 24 %, 5) 16 %. EQE at 1 mA/cm^2: 1) 8 %, 2) 10 %, 3) 7 %, 4) 9 %, 5) 7 %.

b) Radiance versus voltage plots for five TTM-3NCz devices. Radiance levels for EQE_{max} are indicated, and can be distinguished from noise.

c) Current density versus voltage plots for five TTM-3NCz devices.

Figure 5. Device stability for TTM-3NCz.

388 EL spectra for TTM-3NCz devices operated at current densitites between 0.006 and 1.6
389 mA/cm^2. There is no current dependence.

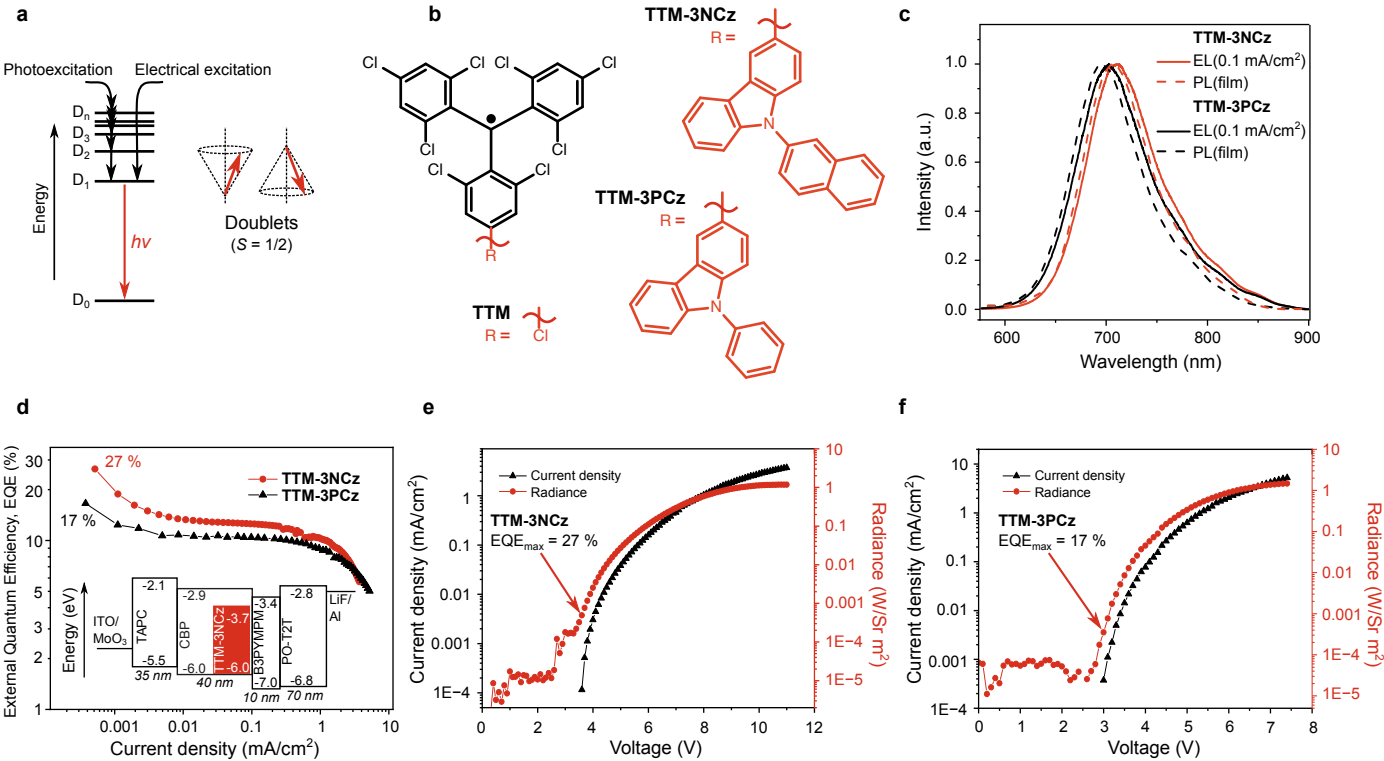
a
Photoexcitation
Electrical excitation
Energy
D_n
D_3
D_2
D_1
D_0
hv
Doublets
(S = 1/2)
b
Cl
R
TTM
R = Cl
TTM-3NCz
R =
TTM-3PCz
R =
N
c
TTM-3NCz
EL(0.1 mA/cm²)
PL(film)
TTM-3PCz
EL(0.1 mA/cm²)
PL(film)
Intensity (a.u.)
Wavelength (nm)
d
27 %
17 %
TTM-3NCz
TTM-3PCz
External Quantum Efficiency, EQE (%)
Current density (mA/cm²)
Energy (eV)
ITO/ MoO3
TAPC
CBP
TTM-3NCz
B3PYMPM
PO-T2T
LiF/ Al
35 nm
40 nm
10 nm
70 nm
e
Current density
Radiance
TTM-3NCz
EQE_max = 27 %
Current density (mA/cm²)
Radiance (W/Sr m²)
Voltage (V)
f
Current density
Radiance
TTM-3PCz
EQE_max = 17 %
Current density (mA/cm²)
Radiance (W/Sr m²)
Voltage (V)

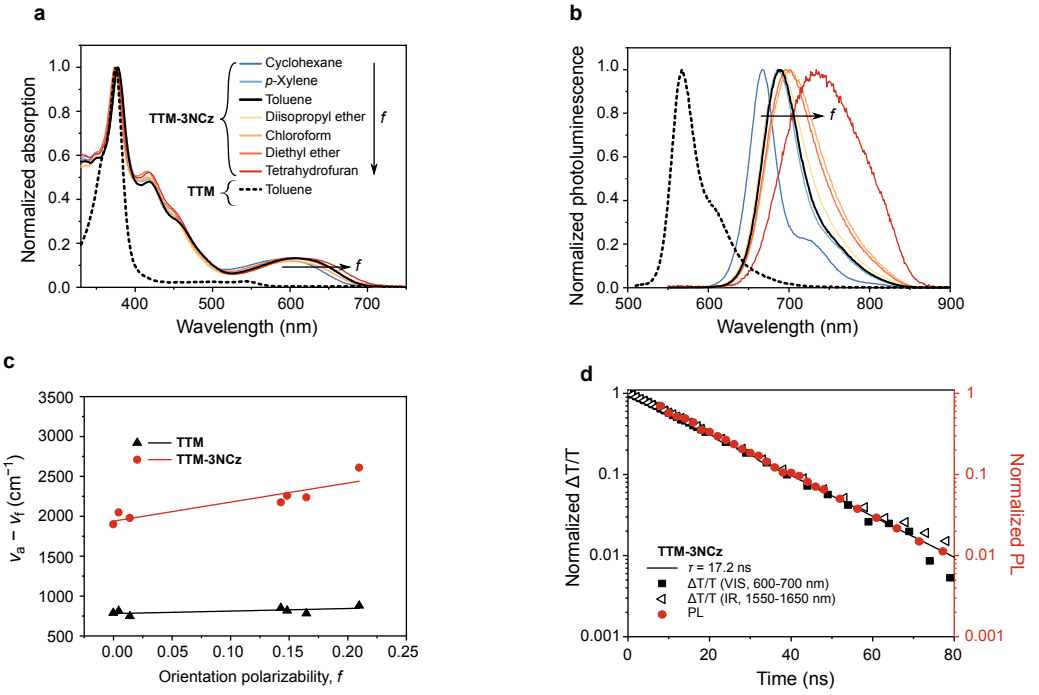
a
Normalized absorption
Wavelength (nm)
TTM-3NCz
Cyclohexane
p-Xylene
Toluene
Diisopropyl ether
Chloroform
Diethyl ether
Tetrahydrofuran
TTM
Toluene
f
b
Normalized photoluminescence
Wavelength (nm)
f
c
$\nu_a - \nu_f$ (cm^{-1})
Orientation polarizability, f
TTM
TTM-3NCz
d
Normalized ΔT/T
Normalized PL
Time (ns)
TTM-3NCz
τ = 17.2 ns
ΔT/T (VIS, 600-700 nm)
ΔT/T (IR, 1550-1650 nm)
PL

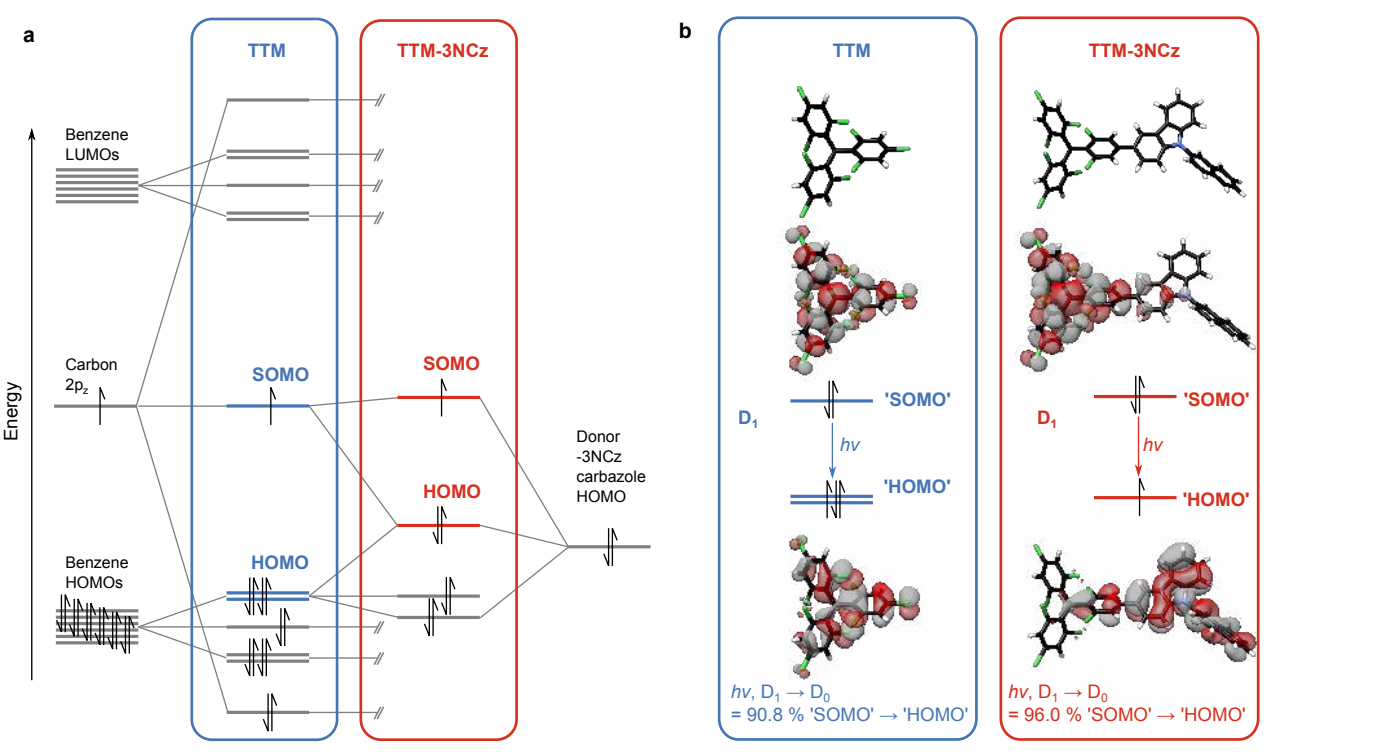
a
TTM
TTM-3NCz
Energy
Benzene
LUMOs
Carbon
2p$_z$
SOMO
SOMO
HOMO
HOMO
Benzene
HOMOs
Donor
-3NCz
carbazole
HOMO
b
TTM
TTM-3NCz
D$_1$
'SOMO'
hv
'HOMO'
D$_1$
'SOMO'
hv
'HOMO'
hv, D$_1$ → D$_0$
= 90.8 % 'SOMO' → 'HOMO'
hv, D$_1$ → D$_0$
= 96.0 % 'SOMO' → 'HOMO'

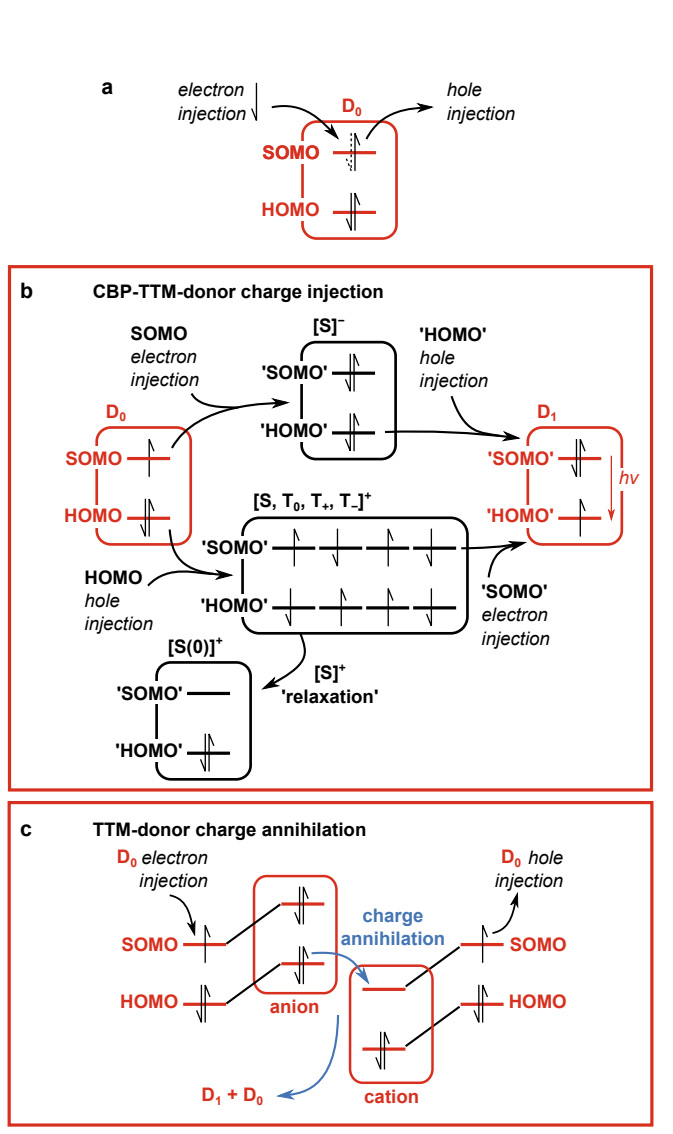
a
electron injection
D0
hole injection
SOMO
HOMO
b
CBP-TTM-donor charge injection
SOMO
electron injection
[S]−
'SOMO'
'HOMO'
'HOMO'
hole injection
D0
SOMO
HOMO
D1
'SOMO'
'HOMO'
hv
[S, T0, T+, T−]+
'SOMO'
'HOMO'
HOMO
hole injection
'SOMO'
electron injection
[S(0)]+
'SOMO'
'HOMO'
[S]+
'relaxation'
c
TTM-donor charge annihilation
D0 electron injection
D0 hole injection
charge annihilation
SOMO
HOMO
anion
SOMO
HOMO
cation
D1 + D0